BEAM-BEAM LIMIT IN A HADRON COLLIDER*

K. Ohmi, KEK, 1-1 Oho, Tsukuba, 305-0801, Japan

Abstract

Beam-beam limit phenomenon is observed in degradation of luminosity lifetime and/or beam lifetime in hadron colliders. We focus the luminosity degradation in LHC. Various effects, which degrade the luminosity, grow severe in high beam intensity. Coherent beam-beam instability, incoherent beam-beam emittance growth and those coupled with lattice errors, external noises, intra-beam scattering are studied. The beam-beam limit in an ideal machine and a machine with above errors is discussed with theory and simulation. Experimental results are reviewed and compare with the theory and simulations.

INTRODUCTION

Beam-beam limit in Hadron colliders has been guessed very low, because the beam oscillation does not damp contrast with lepton colliders. LHC was designed so that the beam-beam parameter is 0.0034 per interaction point at the design stage. Since starting the operation, experiments on the beam-beam effects have been held. There are some sign in which the beam-beam tune parameter is far larger than the design. We try to understand the beam-beam limit in hadron collider, LHC. Possible mechanism limit the beam-beam performance is investigated; ideal machine, crossing angle, offset, IR optics error, IR nonlinearity and external noise in collision offset. Incoherent and coherent phenomena are studied.

BEAM-BEAM LIMIT IN HADRON ACCELERATORS

Parameters of Tevatron, RHIC and LHC are summarized in Table 1. The beam-beam parameter is achieved 0.03 in Tevatron [1]. Tevatron is single ring collider, thus 36 bunches collide with other beam at 136 locations in arc. In LHC, dedicated experiments for a high beam-beam parameter have been held, and the beam-beam parameter 0.034 is achieved without difficulty [2]. In RHIC, tune is constrained between 2/3 and 7/10 to maintain the proton polarization. They try to confine the tune footprint in the constrained area using electron lens [3].

Understanding the beam-beam limit is very important for the design of high luminosity LHC.

We study the beam-beam limit in LHC. Parameters are basically in Table 1, but some of them are E=7 TeV, β^*=0.55m, ε=2.7x10^{-10} m rms ($\gamma\varepsilon$=2.0μm) and bunch population is variable. Though very high bunch population is unphysical, we use it as a control parameter changing the beam-beam tune shift.

Table 1: Summary of Proton Colliders

	Tevatron	RHIC	LHC
Circumf. (m)	6,283	3,834	26,658
Energy (GeV)	980	250	3,500
Emit. (μm)	20(p)/4(pbar)	20	2
beta*	0.28	0.6	1.0
Bunch length (m)	0.48	0.6	0.38
Tune (x/y/z)	20.577/20.570 /0.0007	28.67/29.68 /0.00036	64.31/59.32 /0.0019
Bunch population	2.9x10^{11}(p) 1.1x10^{11}(pbar)	1.65 x10^{11}	1.9x10^{11}
Number of bunches	36	107	1380
Beam-beam parameter	0.03/2IP	0.005/IP	0.034*/2IP
Lumi. (cm^{-2}s^{-1})	4.1x10^{32}	1.45x10^{32}	3.6x10^{33}

* Beam-beam parameter for LHC is obtained in a dedicated experiment [2].

INCOHERENT EMITTANCE GROWTH

Beam particles experience electro-magnetic force induced by the other beam. The force is strongly nonlinear for the transverse amplitude, because the charge distribution of the beam is localized. Betatron amplitude of the beam particles increases in the nonlinear force; that is, emittance growth arises. This emittance growth is not collective, but incoherent phenomenon. The weak-strong model, in which independent beam particles move in a given potential, is available to study the emittance growth.

Simple Model

We first study a simple model consists of round beam collision and linear arc [4].

Beam-beam force for round beam collision is expressed by

$$\Delta p_r = \frac{2N_p r_p}{\gamma}\frac{1}{r}\left[1-\exp\left(-\frac{r^2}{2\sigma_r^2}\right)\right] \qquad (1)$$
$$\Delta p_z = \frac{N_p r_p}{\gamma}\frac{1}{\sigma_r^2}\exp\left(-\frac{r^2}{2\sigma_r^2}\right)\frac{d\sigma_r^2}{dz}$$

Arc is approximated by 6x6 matrix transformation in this model. Simulation is performed by tracking beam particles with repeating Eq.(1) and matrix transformation. Super-periodicity 2 is assumed. Breaking the super-periodicity gives worse results in the most case.

Figure 1 shows luminosity decrement for the simple model. The left plot depicts luminosity evolution in 10^6

turns. The luminosity decrement is estimated by fitting the evolution. The right plot summarizes the luminosity decrement per turn. The revolution frequency is 10^9 per day in LHC. The decrement $\Delta L/L_0=10^{-9}$ corresponds to 1day luminosity lifetime. The beam-beam limit is very high total tune shift $\xi_{tot}>0.2$ for $(\nu_x,\nu_y)=(0.31,0.31)$ and (0.31,0.32). Even in (0.28,0.31), it is $\xi_{tot}>0.1$. For the equal tune, (0.31,0.31), the beam-beam system is approximately one degree of freedom because of $\beta^*> \sigma_z$, thus the very high beam-beam limit is not surprising.

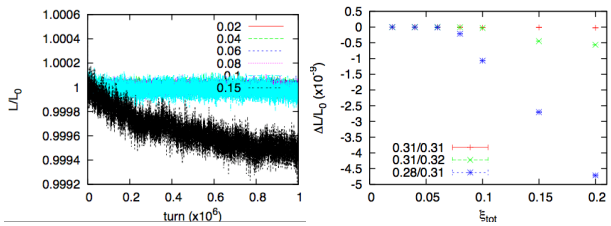

Figure 1: Luminosity decrement for the simple model, which consists of the round beam interaction Eq.(1) and linear arc.

To analyze the mechanism of the luminosity degradation, the frequency map analysis (FMA) [5,6] is performed. The diffusion index is defined by the tune fluctuation as

$$D = \frac{1}{2}\log_{10}(\langle\delta\nu_x\rangle^2 + \langle\delta\nu_y\rangle^2) \quad (2)$$

Figure 2 shows the diffusion index given by FMA. Left and right plots are those in tune space for ξ_{tot} =0.06 and 0.1, respectively. Large fluctuation (~ -4) is seen at x-y coupling in the right bottom edge of the pictures.

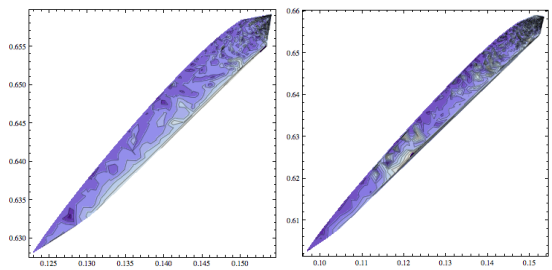

Figure 2: Diffusion index in tune space for the simple model. The contour is every 0.5 step, thus the diffusion index varies -8 to -4 in these plots.

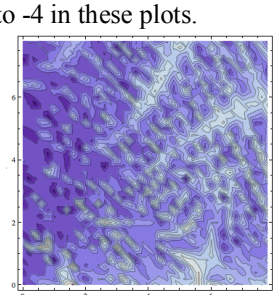

Figure 3: Diffusion index in the amplitude space (x/σ, y/σ) for the simple model. The contour is drawn every 0.5 step.

Crossing Angle and Collision Offset

The crossing angle and collision offset degrade the luminosity performance, since they break symmetry of the collision. Figure 4 and 5 show the luminosity decrement for the crossing and offset collision, respectively. The crossing angle is $\theta_c/2$=143 μrad in half angle; $\theta_c\sigma_z/2\sigma_x$=0.88. The beam-beam limit ($\Delta L/L_0=10^{-9}$) is 0.05 for the crossing collision and is 0.06-0.08 for the offset collision.

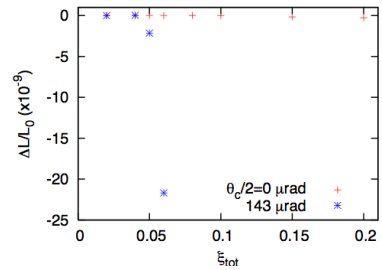

Figure 4: Luminosity decrement for collision with or without crossing angle, 143 μrad in half angle.

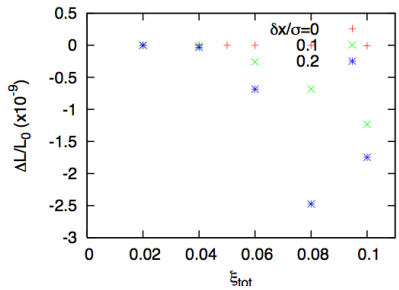

Figure 5: Luminosity decrement for collision with horizontal offset, 0, 10 and 20% of the beam size.

Figures 6 and 7 show results of the FMA. For the horizontal crossing collision, horizontal tune shift is smaller than vertical, therefore the strong coupling resonance is seen, but the resonance does not contribute the emittance growth; (0.31,0.32) is better than (0.305,0.32). For both of the crossing and offset collisions, 7-th order and 13-th order resonances are seen. 7-th order resonances are (m_x, m_y)=(7,0), (5,2), (3,4) and (1,6), where $m_x\nu_x + m_y\nu_y$=n. 13-th order resonances arise large amplitude, thus it does not contribute to the emittance growth.

Figure 8 shows the phase space plot in x-p_x for crossing and offset collisions. As is expected, 7 islands are seen. The diffusion index and resonance width is similar for crossing and offset collisions, while the emittance growth rate for the crossing collision is stronger than that of the offset collision. We discuss the difference in the subsection of the synchrotron motion.

ISBN 978-3-95450-115-1

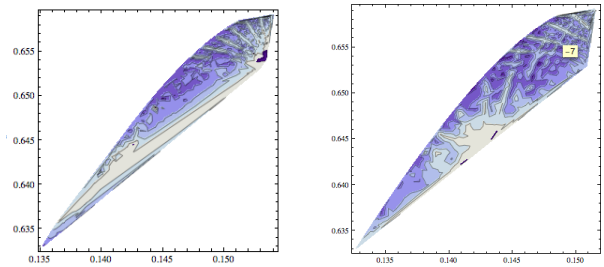

Figure 6: Diffusion index for the crossing collision. Left and right pictures are drawn for the bare tune (0.31,0.32) and (0.305,0.32). The contour is every 1 step, thus the diffusion index varies -8 to -3 in these plots.

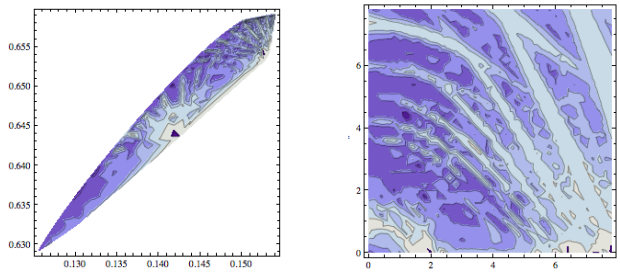

Figure 7: Diffusion index for offset collision of 20% σ. Left and right pictures are drawn in tune and amplitude spaces. The contour is every 1 step, thus the diffusion index varies -8 to -3 in these plots.

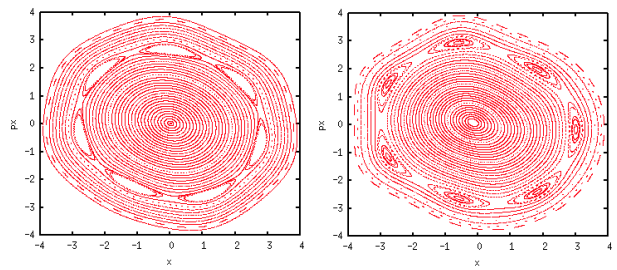

Figure 8: Phase space (x-p_x) plot for the crossing (left) and offset (right) collision.

The resonances are studied by Taylar map analysis. The map is factorized by

$$\mathcal{M} = M \exp(-:H:) \tag{3}$$

where M is linear map including linear beam-beam tune shift, and H is nonlinear map higher than 3rd order polynomials. H is expressed by the action variables, J_i and ϕ_i, i=x,y. Fourier component is defined by

$$H = H_{00} + \sum G_{m_x,m_y} \exp(m_x\phi_x + m_y\phi_y) \tag{4}$$

Taylar map for the crossing collision up to 12-th order is obtained and the Fourier component is given as follows,

$$\begin{aligned} H_{00}(J_x,J_y) = {} & 2.01375\times10^{42}J_x^6 + 1.21356\times10^{43}J_x^5J_y - 4.82225\times10^{43}J_x^5 \\ & +2.79527\times10^{43}J_x^4J_y^2 - 2.2716\times10^{34}J_x^4J_y + 1.14155\times10^{25}J_x^4 \\ & +1.29819\times10^{44}J_x^3J_y^3 - 7.27118\times10^{34}J_x^3J_y^2 - 4.63551\times10^{25}J_x^3J_y \\ & -2.70542\times10^{16}J_x^3 - 1.66781\times10^{44}J_x^2J_y^4 - 1.48894\times10^{36}J_x^2J_y^3 \\ & +1.18738\times10^{26}J_x^2J_y^2 - 8.66053\times10^{16}J_x^2J_y + 6.10249\times10^{7}J_x^2 - 1.79409\times10^{44}J_xJ_y^5 \\ & -1.71884\times10^{35}J_xJ_y^4 + 1.68734\times10^{26}J_xJ_y^3 - 1.57801\times10^{17}J_xJ_y^2 - 1.36494\times10^{8}J_xJ_y \\ & +1.07216\times10^{44}J_y^6 - 1.2051\times10^{35}J_y^5 + 1.3982\times10^{26}J_y^4 - 1.59505\times10^{17}J_y^3 \\ & +1.74099\times10^{8}J_y^2 \end{aligned} \tag{5}$$

$$\begin{aligned} G_{70}(J_x,J_y) = {} & -(1.02037\times10^{36} + 3.66357\times10^{37}i)J_x^{7/2}J_y^2 \\ & -(9.42572\times10^{35} + 2.37993\times10^{37}i)J_x^{9/2}J_y \\ & +(6.12286\times10^{26} + 1.98798\times10^{28}i)J_x^{7/2}J_y \\ & +(-3.22114\times10^{35} - 5.54337\times10^{36}i)J_x^{11/2} \\ & +(3.8924\times10^{26} + 1.0181\times10^{28}i)J_x^{9/2} \\ & -(2.88738\times10^{17} + 1.01787\times10^{19}i)J_x^{7/2} \end{aligned} \tag{6}$$

$$\begin{aligned} G_{52}(J_x,J_y) = {} & -(5.21869\times10^{36} + 1.9088\times10^{38}i)J_x^{5/2}J_y^3 \\ & -(1.83356\times10^{36} + 1.65091\times10^{38}i)J_x^{7/2}J_y^2 \\ & +(2.9534\times10^{27} + 1.20767\times10^{29}i)J_x^{5/2}J_y^2 \\ & +(-1.84853\times10^{36} - 4.61116\times10^{37}i)J_x^{9/2}J_y \\ & +(2.16367\times10^{27} + 6.78959\times10^{28}i)J_x^{7/2}J_y \\ & -(1.47942\times10^{18} + 5.8524\times10^{19}i)J_x^{5/2}J_y \end{aligned} \tag{7}$$

$$\begin{aligned} G_{34}(J_x,J_y) = {} & (-9.67426\times10^{36} - 3.4081\times10^{38}i)J_x^{3/2}J_y^4 \\ & -(1.05055\times10^{37} - 3.63976\times10^{38}i)J_x^{5/2}J_y^3 \\ & +(6.18733\times10^{27} - 2.27764\times10^{29}i)J_x^{3/2}J_y^3 \\ & -(3.63487\times10^{36} - 1.19293\times10^{38}i)J_x^{7/2}J_y^2 \\ & +(3.73778\times10^{27} - 1.46504\times10^{29}i)J_x^{5/2}J_y^2 \\ & -(2.66418\times10^{18} - 1.07435\times10^{20}i)J_x^{3/2}J_y^2 \end{aligned} \tag{8}$$

$$\begin{aligned} G_{16}(J_x,J_y) = {} & -(8.32095\times10^{36} + 2.71833\times10^{38}i)J_x^{3/2}J_y^4 \\ & -(3.54179\times10^{36} - 1.15319\times10^{38}i)J_x^{5/2}J_y^3 \\ & +(3.13206\times10^{27} - 1.0905\times10^{29}i)J_x^{3/2}J_y^3 \\ & +(-5.92947\times10^{36} - 2.01088\times10^{38}i)\sqrt{J_x}J_y^5 \\ & +(3.70417\times10^{27} - 1.37856\times10^{29}i)\sqrt{J_x}J_y^4 \\ & -(1.61398\times10^{18} - 6.33474\times10^{19}i)\sqrt{J_x}J_y^3 \end{aligned} \tag{9}$$

The resonances in amplitude space and their width are given by

$$m_x\left(\nu_{x0} + \left.\frac{\partial H_{00}}{\partial J_x}\right|_{J=J_R}\right) + m_y\left(\nu_{y0} + \left.\frac{\partial H_{00}}{\partial J_y}\right|_{J=J_R}\right) = n \tag{10}$$

and

$$\Delta J_x = 2m_x\sqrt{\frac{G_{m_x,m_y}}{\Lambda}} \tag{11}$$

where

$$\Lambda = m_x^2\frac{\partial^2 H_{00}}{\partial J_x^2} + m_xm_y\frac{\partial^2 H_{00}}{\partial J_x\partial J_y} + m_y^2\frac{\partial^2 H_{00}}{\partial J_y^2}$$

Figure 10 shows the resonance lines in the amplitude space. The lines well agree with the FMA result in Figure 7.

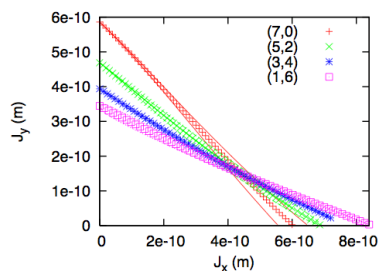

Figure 10: Resonance lines in the amplitude space given by Taylar map analysis.

Synchrotron Motion

Figure 11 shows the luminosity evolution with and without synchrotron motion. The decrement strongly depends on the synchrotron motion [4]. Figure 12 shows the luminosity decrement as a function of the beam-beam

parameter for crossing and offset collision. Both are similar results. The decrement contrasts with that with synchrotron motion in Figure 4.

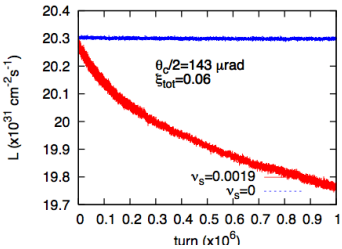

Figure 11: Luminosity evolution for the arc transformation with or without synchrotron oscillation.

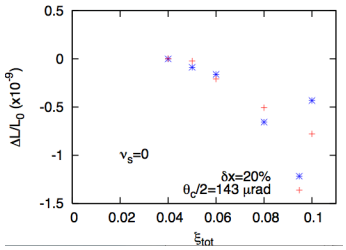

Figure 12: Luminosity decrement for offset or crossing collision at ν_s=0.

IR coupling, dispersion and chromaticity

x-y coupling and dispersion at IP strongly degraded the luminosity performance in a flat beam collision, for example in KEKB. The effect is weak for LHC, because of the round beam. Some simulation results are seen in Ref. [7].

IR Nonlinearity

The final triplet in the interaction region The quadrupole magnets are located at very high beta section. The dynamic aperture is mainly limited by the nonlinearity of the IR magnets. We use IR model [8] for the beam-beam simulation. Figure 13 shows that the nonlinearity degrades luminosity at high beam-beam parameter ξ>0.1. FMA analysis shown in Figure 14 indicates 10-th order resonances (1,9), (3,7), (5,5), (7,3) and (9,1).

Beam Loss Due to Long Range Beam-Beam Force

The dynamic aperture of the IR model roughly reproduces that of whole ring. Beam loss due to long range beam-beam force can be simulated using the IR model as is presented in this talk.

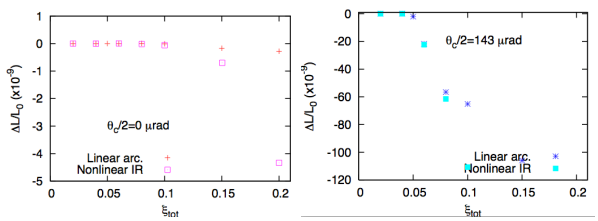

Figure 13: Luminosity decrement for linear arc and nonlinear IR.

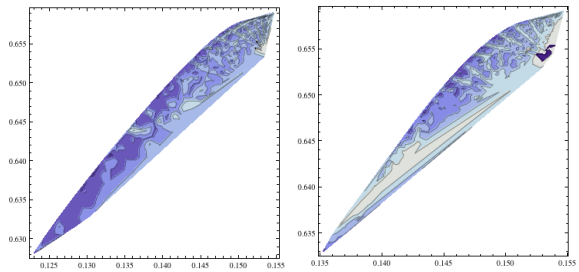

Figure 14: Diffusion index for IR model. θ_c/2=0(left) and 143 μrad (right).

Incoherent Emittance Growth in a Strong-Strong Simulation

The emittance growth has been studied also using a strong-strong simulation code, named BBSS. The simulation is performed for the number of macro-particles, 10^6 and $2x10^6$. Statistics of macro-particles induces an offset fast noise, which results artificial luminosity decrement. Degradation (difference) due to a static collision offset (10%) in Figure 5 is seen.

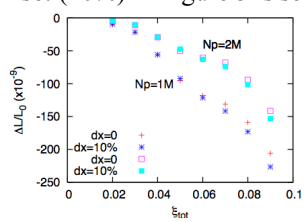

Figure 15: Luminosity decrement by a strong-strong simulation.

COHERENT INSTABILITY

Coherent instability is studied by the strong-strong simulation (BBSS). Keeping horizontal tune, vertical tune is scanned. Luminosity degradation is seen at near integer, half-integer and 59.36. The instability ~59.36 is enhanced by collision offset. Frequency spectra near ν_y~0.36 are shown in Figure 17. Clear signal for the mode coupling between dipole π mode and quadrupole mode is seen [9].

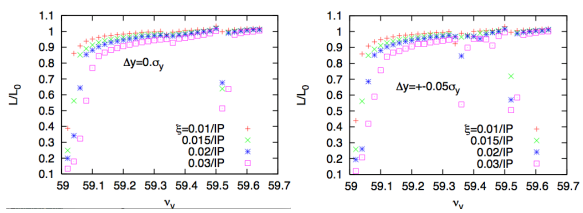

Figure 16: Luminosity degradation scanning tune.

NOISE

Coherent Random Noise for Collision Offset

Fast noise in collision offset degrades the luminosity performance. The strong-strong simulation showed emittance growth due to the macro-particle statistics, though it is artifact. The offset collision induces a small

ISBN 978-3-95450-115-1

coherent motion. Damping or smearing of the coherent motion results in an emittance growth [10,11,12]. The growth rate is expressed by [11] where K=0.089, and G is damping rate of the coherent motion.

$$\frac{\delta\varepsilon}{\varepsilon} \approx \frac{K}{\left(1+\frac{G}{2\pi|\xi|}\right)^2}\frac{\delta x^2}{\sigma_x^2} \qquad (12)$$

In the analytic theory, the beam-beam system is assumed approximately solvable.

Figure 18 shows luminosity decrement for the noise amplitude. Left and right plots are without and with crossing angle. The decrement is quadratic for the noise amplitude and scale for ξ^2. The simulations give K~0.023-0.4 for G=0-1. In the simulation, offset noise is turn-by turn, that is, G=1 for the strong beam, while G=0 for the weak beam. Figure 19 shows luminosity decrement as a function of the beam-beam parameter under an offset noise. The tune shift is reduced to 70% for the crossing collision. The luminosity decrement for noise is independent of the crossing angle. At higher beam-beam parameter >0.05, the luminosity decrement due to crossing angle is dominant.

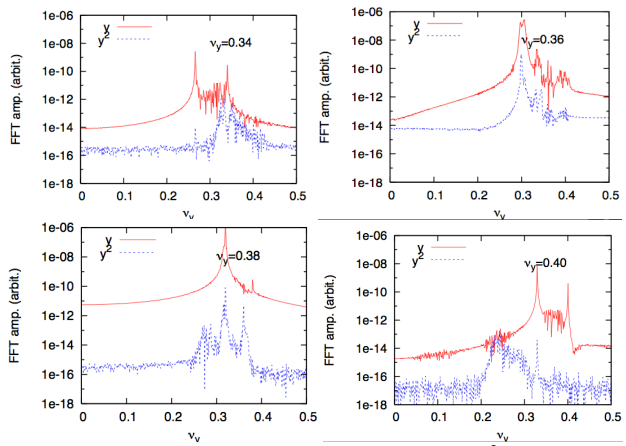

Figure 17: Frequency spectra for <y> and <y^2>. The four plots depict the spectra for tunes, 0.34, 0.36, 0.38 and 0.40.

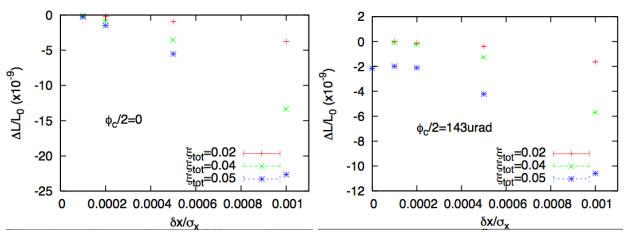

Figure 18: Luminosity decrement for noise amplitudes.

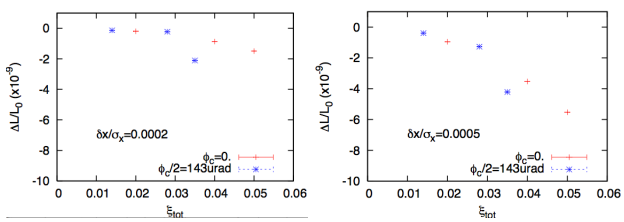

Figure 19: Luminosity decrement as a function of the beam-beam parameter under an offset noise.

Incoherent Noise Due to Intra-Beam Scattering

Emittance growth due to intra-beam scattering (IBS) is 105 h and 63 h for the horizontal and longitudinal, respectively, in the nominal LHC [13]. The transverse emittance and bunch population in the nominal are $5.0\text{x}10^{-10}$ and $1.15\text{x}10^{11}$, respectively. The horizontal IBS growth rate is approximately proportional to the particle density in the six dimensional phase space. The growth time is 40 h for ξ_{tot}=0.02 in this paper ($\varepsilon=2.7\text{x}10^{-10}$ and $N_p=1.63\text{x}10^{11}$). The fluctuation is $\delta x/\sigma_x=5.5\text{x}10^{-5}$ for ξ_{tot}=0.05 (16h). The luminosity decrement is determined by geometrical emittance growth $\delta L/L=1/2\ \delta x^2/\sigma_x^2$ for incoherent noise.

SUMMARY

We discuss the beam-beam limit in LHC with every possible mechanism. The results show a hurdle ξ_{tot} ~0.05 for offset or crossing. They are consistent with experimental result at the present.

ACKNOWLEDGMENT

The author thanks Drs. Y. Alexahin, W. Fischer, W. Herr, R. Tomas, A. Valishev, D. Zhou, F. Zimmermann.

REFERENCES

[1] E.G. Stern et al., Phys. Rev. ST-AB. 13 (2010) 024401.
[2] W. Herr, presentation given in Chamonix workshop 2012.
[3] W. Fischer et al., ICFA Beam Dynamics Newslett, 52 (2010) 102.
[4] K. Ohmi, K. Oide, Phys. Rev. ST-AB. 10 (2007) 014401.
[5] L. Nadolski, J. Laskar, Phys. Rev. ST-AB, 6 (2003), 114801.
[6] D. Shatilov et al. Phys. Rev. ST-AB, 14 (2011), 014001.
[7] K. Ohmi, Proceedings of workshop on "The High -Energy Large Hadron Collider", Malta, Oct. 2010, CERN-2011-003, p. 93 (2011).
[8] K. Ohmi, H. Koiso, IPAC2010, Kyoto, (2010).
[9] Y. Alexahin, Nucl. Instru. Methods in Phys. Res., A480 (2002) 253.
[10] T. Sen and J.A. Ellison, Phys. Rev. Lett. 77 (1996) 1051.
[11] Y. Alexahin, Nucl. Instru. Methods in Phys. Res., A391 (1996) 73.
[12] K. Ohmi et al., "Beam-beam effect with an external noise in LHC", PAC'07, Albuquerque, June, 2007, TUPAN048, p. 1496 (2007); http://www.JACoW.org
[13] LHC design report, CERN-2004-003-V-1; http://lhc.web.cern.ch/lhc/lhc-designreport.html